Asian Journal of Chemistry; Vol. 34, No. 6 (2022), 1517-1525

ASIAN JOURNAL OF CHEMISTRY

https://doi.org/10.14233/ajchem.2022.23689

Study of Antiviral Activity of Some Pyrimidine Ring Containing Compounds against COVID-19 Based on Molecular Docking and Quantum Chemical Calculations by DFT Method

S. Helen, M.A.K. Liton*, M. Das and Md. Nuruzzaman

Department of Chemistry, Faculty of Science, Mawlana Bhashani Science and Technology University, Santosh, Tangail-1902, Bangladesh

*Corresponding author: Tel: +8801815-473028; E-mail: aklitonchemmbstu@gmail.com

Received: 21 December 2021; *Accepted*: 14 March 2022; *Published online*: 18 May 2022; AJC-20816

The novel coronavirus, COVID-19, caused by SARS-CoV-2, is a global health pandemic and currently no specific drug is available to prevent or cure this novel coronavirus (SARS-CoV-2) disease. We have been put forth five pyrimidine ring containing compounds as potential antiviral candidatures for the treatment of COVID-19 diseases based on quantum chemical properties predicted by molecular docking study and DFT calculations at the level of B3LYP method with 6-311++G (d,p) basis set. Our findings were also compared to remdesivir, a control ligand. Blind docking with the main protease revealed that the ligands preferentially bind to the active site. Interestingly, all of the ligands exhibited low binding free energies *i.e.*, strong inhibitory interactions with the active sites of the main protease. Ligand **L1** was one of them, which revealed significantly low binding energies (-8.8 kcal/mol) with SARS-CoV-2 M^{pro}. These binding energies are even lower than those of remdesivir's potent active metabolite. All of the drugs interact with the key active site residues, including His41 and Cys145. These findings are also strongly supported by quantum chemical investigations.

Keywords: COVID-19, Pyrimidine ring, HOMO-LUMO, Molecular docking, DFT calculations.

INTRODUCTION

A typical pneumonia cases were reported to the World Health Organization (WHO) on December 31st, 2019, in Wuhan City (Hubei Province), China [1]. Every day, a large number of people die as a result of this devastating disease. By November 8, 2021, the total number of COVID-19 cases and deaths had reached 250,774,454 and 5,067,764, respectively. The COVID-19 pandemic is continuing strongly and the SARS-CoV-2 virus has been confirmed in 222 countries and territories around the world. The emergence of the highly transmissible disease SARS-CoV-2 has given birth to the pandemic COVID-19, provoking widespread fear and considerable impact on the world economy [2-4]. To date, hand hygiene, self-isolation of sick individuals, isolation, global travel limitations, shutdowns and physical separation have been the only options for preventing the spread of disease, all of which have serious health, social and economic consequences [5]. There are currently no particular treatments available for COVID-19 and patient's treatment options are restricted to medications that can alleviate symptoms [6]. A number of drug treatments have been proposed all around the world. Antiviral like α-ketoamides has also been described as inhibitors of the coronavirus main protease in the literature [7]. Other antiviral drugs, including remdesivir, lopinavir, ritonavir and interferon α, have also been suggested as prospective treatment alternatives against COVID-19 [8].

The framework spike (S) glycoprotein, envelop (E), membrane (M), nucleocapsid (N), hemagglutinin esterase dimer (HE) and non-structural proteins (NSP) are among the structural and non-structural proteins found in SARS-CoV-2 [9]. The main protease enzyme M^{pro} of SARS-CoV-2 is a homodimer that plays a crucial role in viral replication, making it a promising target for finding SARS-CoV-2 inhibitors [6]. Protease inhibitors could likely block a crucial enzyme that assists viruses in replicating and prevents SARS, which is also a coronavirus [10]. Coronaviruses (CoVs) are enveloped viruses, having a single-stranded, positive-sense RNA genome. They are giant spherical viruses with a diameter of 80-120 nm and a crown-like appearance due to glycoprotein spikes [11]. Due to its 82% similarity to the SARS coronavirus (SARS-CoV), the virus has been named SARS-CoV-2 [12]. A catalytic dyad comprising His41 and Cys145 is found in the active site of the enzyme [13].

Nowadays, computer-aided drug design (CADD) techniques such as pharmacophore modeling, virtual screening, molecular docking and dynamic simulation are widely utilized to find, create and assess drugs and other physiologically active compounds [14]. A structure-based computational technique for anticipating the complementarity between a drug ligand and a therapeutic target is known as molecular docking [15]. The increased demand for computational drug discovery methodologies is driven by the urgent need for new drugs to control SARS-CoV-2 [16].

In this regard, a well-ordered quantum chemical study of the feasible conformations and their relative stabilities has been performed in this work. Density functional computations utilizing B3LYP at 6-311++G(d,p) basis set were executed by applying Gaussian 09 suit program. In this context, at first, geometric optimization of the proposed compounds have done successfully using B3LYP method at the 6-311++G (d,p) level of theory. Then their reactivity and behaviours were predicted at the same level of theory by using thermal parameters, frontier molecular orbitals, molecular electrostatic potentials and Mullikens atomic charges. Some of the important electronic properties such as ionization potential, electron affinity, dipole moment, polarizability, chemical hardness, chemical softness, electronegativity, chemical potential, electrophilicity index and maximum charge transfer index were also determine so as to find out the most reactive compounds against the COVID-19 virus. Most of these properties are use in quantitative structural analysis relationship (QSAR) and drug design [17-19].

In addition, this study also assesses the binding mode of compounds to proteins using molecular docking simulation. We used a molecular docking study to examine the binding affinity of the five compounds (**L1-L5**) towards the SARS-CoV-2 main protease (M^{pro}) and compared the results to an FDA-approved drug, remdesivir. As a result, this study would be used as a future guideline to develop novel drugs for treating COVID-19 patients.

COMPUTATIONAL METHODS

Gaussian 09W software package has been employed for all the theoretical calculations [20]. Geometry optimization of the studied ligands were executed by using DFT (density functional theory) at B3LYP/6-311++G (d,p) level of theory [21-24]. The molecular structure of the optimized ligands was visualized by Gauss View 6.0.16 software [25]. FMOs orbitals, electronic properties, molecular electrostatic potential surfaces (MEP_S) and Mulliken atomic charges were determined at the same level of theory. PyRx AutoDock Vina Wizard [26] was used to calculate the binding affinity and to identify what type of interactions occur between ligands and targets (PDB ID: 6Y2G) during molecular docking studies. The PyMol software package (version 2.4.0) [27] was used to prepare protein structures. The substrates or protein macromolecules were treated as the rigid target, whereas the ligands were treated as flexible targets with various rotatable bonds.

Preparation of protein, ligands optimization and molecular docking: For molecular docking simulations, the X-ray crystallographic structure of SARS-CoV-2 M^{pro} (PDB ID: 6Y2G) was obtained from the RCSB Protein Data Bank at a structural resolution of 2.20 Å [28]. After that Swiss-PDB viewer software package (version 4.1.0) was used to optimize and check the crystal structure of the M^{pro} based on their least energy [29]. The PyMol (version 2.4.0) software package was used to construct the protein structure for docking. This phase entailed removing all heteroatoms, water molecules and inhibitors from the structure and adding missing hydrogens to the receptor. The 3D structures of all the compounds were created using the Gauss View 6.0. 16 software and geometry optimization was performed using Gaussian 09 W program at the B3LYP/6-311++ G (d,p) level of DFT (Fig. 1).

Blind docking was performed using AutoDock Vina after ligand and protein preparation. The receptor grid covered the entire protein, where the centre was X: -8.4137, Y: 6.6830, Z:

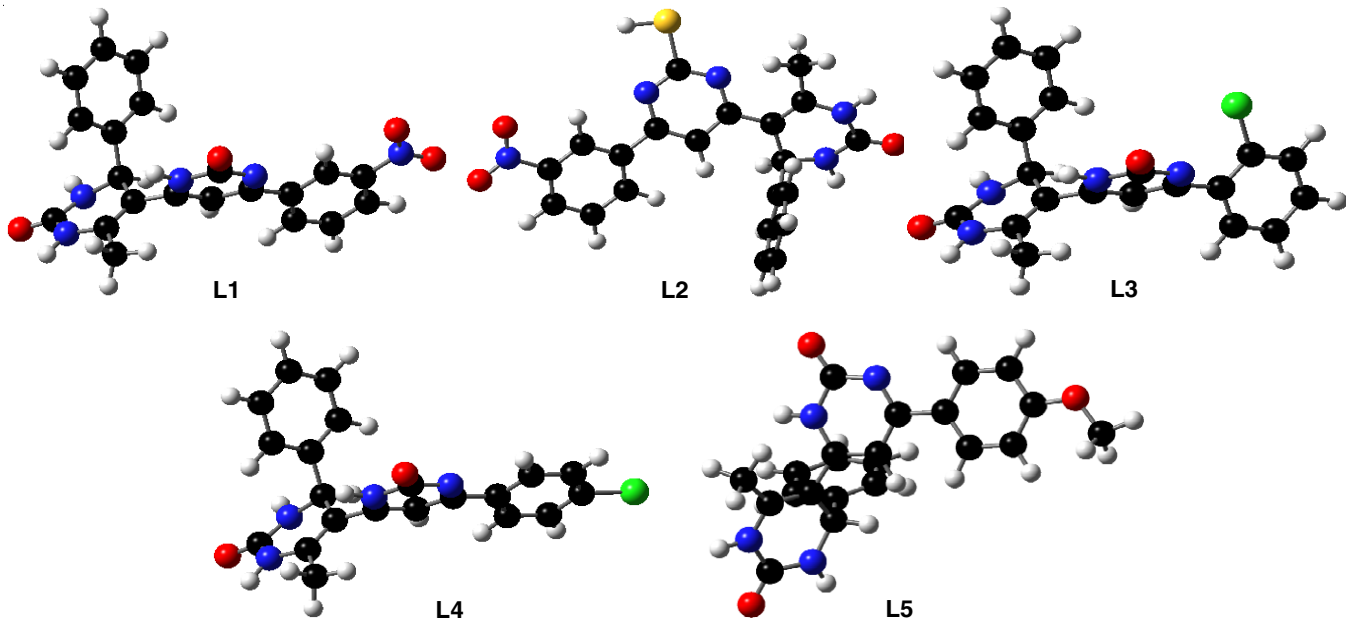

Fig. 1. Optimized structures of the studied ligands (**L1-L5**) by using DFT/B3LYP/6-311++G (d,p) method

-26.8964 and the dimensions were X: 77.1451, Y: 39.3223 and Z: 51.8757. The binding affinities of the ligands were measured as negative scores in kcal/mol unit, with higher negative values indicating higher binding affinities. PyRx virtual screening software was used to execute the docking simulations, which used the AutoDock Vina docking protocol [26]. PyMol (version 2.4.0), BIOVIA Discovery Studio (version 4.5) and Chimera X-1.1 [30] were used to visualize the docking results and non-covalent interactions in the docked ligand-protein complex. Graphical representations of the docked pose were created using the Chimera X-1.1 program.

RESULTS AND DISCUSSION

DFT calculation studies: To explore the electronic structure of a compound and also to investigate the interactions involved between the receptors and ligands computational quantum mechanical modeling method DFT is very useful tool [31]. Dipole moment and polarizability are important factors that are related to the polarity of a molecule and provides information about charge distribution within the molecule and therefore play important role in solvation, binding affinity, inhibition activity, molecules membrane permeability system [32,33]. In addition, they exhibit significant contribution in protein-ligand and drug-receptor interactions [34]. This may be due to the propagation of an electrostatic field by the receptor and therefore would attack more strongly and interact with molecules, which have a higher dipole moment or polarizability [35]. Hence, molecules, which have large dipole moment and polarizability, that molecules will show high inhibition activity and binding affinity. DFT/B3LYP/6-311++G(d,p) level of theory executed total energy, thermal parameters, dipole moment and polarizability of the studied ligands are presented in Table-1. It is observed that all studied ligands **L1-L5** show considerable amount of dipole moment change and large polarizability value. That means all studied ligand could set out their binding pose within a specific target protein. Among them, **L1** show high dipole moment and **L2** show large polarizability than other ones. Hence, their binding affinity will be excellent than other ones.

Thermodynamic parameters are very important to gain insight into the balance of energetic forces driving interactions and to access molecular interactions [36]. Free energy is the most inevitable parameter that provides information about the interaction of binding partners and whose magnitude and sign also give indication about the possibility of biomolecular events occurring. Free energy is composed of enthalpy and entropy. Therefore, they have direct contribution in molecular forces governing binding system [37]. Molecules higher binding affinity rely on large negative value of G. Since all the studied ligands show large negative G value, thus their binding affinity will be good and might act as good inhibitor against SARS-CoV-2.

Frontier orbitals and quantum chemical calculations: The energies of HOMO, LUMO orbitals and chemical reactivity descriptors of studied ligands were calculated by using DFT at B3LYP/6-311++ G (d,p) level of theory and tabulated in Table-2. Ionization energy (I) and electron affinity (A) of the studied ligands were determined by using HOMO and LUMO energies. A large energy gap between HOMO and LUMO energies indicates the lower reactivity, while a small energy gap indicates higher reactivity. The FMOs results analysis of the studied ligand showed that energy gap decreases in the following order: **L1 > L2 > L4 > L5 > L3**. Thus, the order of reactivity of the studied ligand increases according to the following **L1 > L2 > L4 > L5 > L3** (Fig. 2). These results are in good agreement with the molecular docking results. The chemical hardness (η) and softness (σ) of a molecule also depend on the how much easier an electron flow from HOMO to LUMO. Hence, small energy gap makes a molecule softer and more reactive, while large energy gap makes harder and less reactive. Since ligand **L1** has higher chemical softness value than other ligands, thus ligand **L1** will be more reactive than other ligands. Negative chemical potential (μ) of the studied ligand implies that all are stable and form stable complex with the protein. Electronegativity (χ) value is an indication of the power of the molecule to attract electrons. Global electrophilicity index (ω) also measures the tendency of a species to accept an electron [38]. Good electrophiles can be taken into account when the values of μ and ω are high. Lastly, the proportion of maximum charge that a system can acquire from its environment is represented by maximum charge transfer index (ΔN_{max}). From Table-2, it is observed that the electronegativity and electrophilicity index of the studied ligand increases in the following order: **L1 > L2 > L4 > L3 > L5**. Maximum charge transfer index (ΔN_{max}) also follow the same order. Based on the value found from HOMO, LUMO energies, energy gap and chemical reactivity descriptors, it is concluded that ligand **L1** will show high reactivity and could

TABLE-1
CALCULATED TOTAL ENERGY (Hartree/particle), THERMAL PARAMETERS (kcal/mol), DIPOLE MOMENT (debye) AND POLARIZABILITY (a.u.) OF THE STUDIED LIGANDS (**L1-L5**) BY BY USING DFT/B3LYP/6-311++G(d,p) LEVEL OF THEORY

Parameter	L1	L2	L3	L4	L5
E_{total}	-1385.446849	-1708.407939	-1640.499555	-1640.508904	-1295.443990
E_0	-869157.60	-1071822.33	-1029213.24	-1029218.96	-812661.11
E	-868917.61	-1071585.49	-1028981.62	-1028987.22	-812402.26
H	-868917.02	-1071584.90	-1028981.03	-1028986.62	-812401.67
G	-868971.18	-1071639.00	-1029032.65	-1029038.19	-812455.67
Dipole moment	7.5303	4.2668	4.1899	3.3763	5.0645
Polarizability	311.3336	337.3846	298.7376	311.7026	319.1913

E_0: Sum of electronic and zero-point energies ($E_0 = E_{elec} + ZPE$), E: Sum of electronic and thermal energies ($E = E_0 + E_{vib} + E_{rot} + E_{trans}$), H: Sum of electronic and thermal enthalpies (H = E + RT), G: Sum of electronic and thermal free energies (G = H - TS).

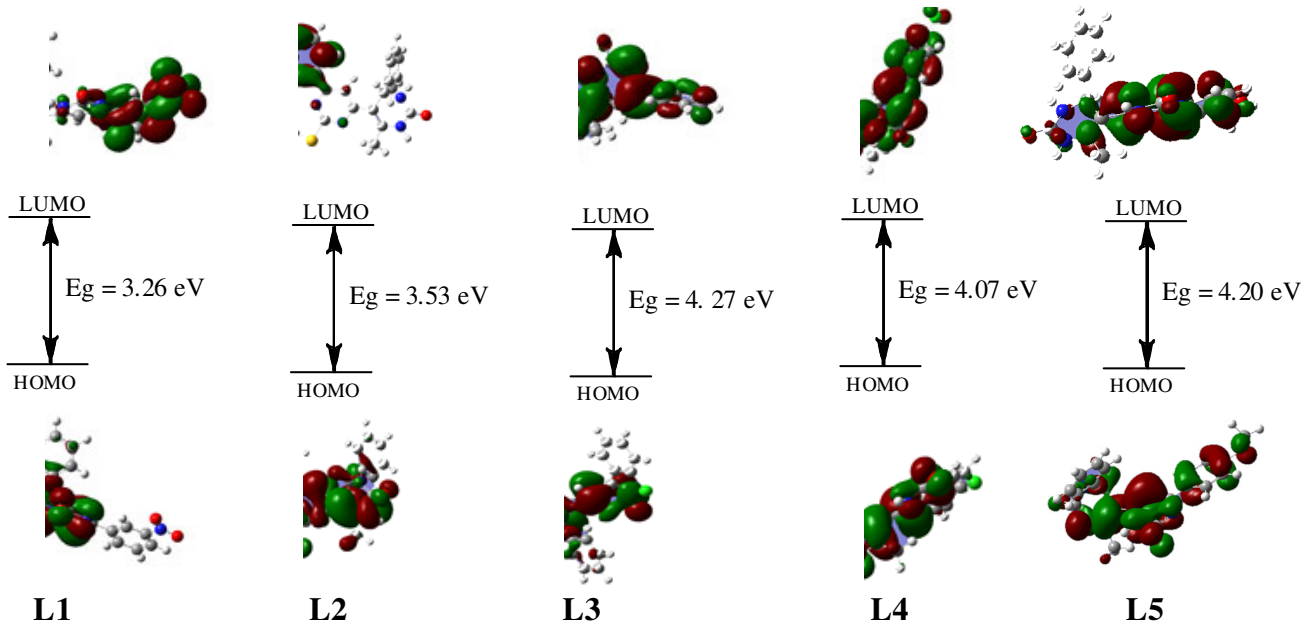

Fig. 2. HOMO and LUMO plots for all studied ligands calculated at B3LYP/6-311++G (d,p) level of theory

TABLE-2
CALCULATED E_{HOMO}-E_{LUMO} GAP VALUES, IONIZATION POTENTIAL (I), ELECTRON AFFINITY (A), CHEMICAL HARDNESS (η), CHEMICAL SOFTNESS (σ), ELECTRONEGATIVITY (χ), CHEMICAL POTENTIAL (μ), ELECTROPHILICITY INDEX (ω) AND MAXIMUM CHARGE TRANSFER INDEX (ΔN_{max}) OF THE STUDIED LIGANDS AT DFT/B3LYP/6-311++G (d,p) LEVEL OF THEORY

Parameters	L1	L2	L3	L4	L5
E_{HOMO} (eV)	-6.42	-6.51	-6.51	-6.54	-6.34
E_{LUMO} (eV)	-3.16	-2.98	-2.24	-2.47	-2.14
Energy gap	3.26	3.53	4.27	4.07	4.20
Reactivity descriptors					
Ionization potential (I)	6.42	6.51	6.51	6.54	6.34
Electron affinity (A)	3.16	2.98	2.24	2.47	2.14
Chemical hardness (η)	1.63	1.76	2.13	2.03	2.10
Chemical softness (σ)	0.81	0.88	1.06	1.01	1.05
Electronegativity (χ)	4.79	4.74	4.37	4.50	4.24
Chemical potential (μ)	- 4.79	- 4.74	- 4.37	- 4.50	- 4.24
Electrophilicity index (ω)	7.03	6.38	4.48	4.99	4.27
Maximum charge transfer index (ΔN_{max})	2.93	2.69	2.05	2.21	2.01

$I = - E_{HOMO}$, $A = - E_{LUMO}$, $\eta = (I - A)/2$, $\sigma = 1/2\ \eta$, $\chi = (I + A)/2$, $\mu = - (I + A)/2$, $\omega = \mu^2/2\ \eta$ and $\Delta N_{max} = - \mu/\eta$.

facilitate the binding with the targeted protein. These results show the good compatibility with those obtained by molecular docking.

Molecular electrostatic potential (MEP): In this study, mapped MEP surfaces were obtained for five ligands (**L1-L5**) by using the checkpoint file after optimization utilizing Gaussian 09 program along with B3LYP/6-311++G (d,p) level of theory. In Fig. 3, most negative, most positive and zero potential regions are visualized by red, blue and green colour and these colour grading act as an indicator of molecular structural properties of the ligands under investigation. Most electronegative electrostatic potential is represented by red colour. Thus, this region will be most preferred sites for electrophilic attack. Most electropositive potential is signified by blue colour. Thus, this region will be most preferred sites for nucleophilic attack.

It is observed that in the MEP map of all studied ligands **L1-L5** (Fig. 3), the red colourations, which indicate nucleophilic sites, are localized on the O atoms of C=O bond. The red colourations are also observed on the O atoms of N=O bond for **L1** and **L2**. On the other hand, the blue colours, indicative of electrophilic sites are observed on the N-H bond. In all ligands (**L1-L5**), due to the different positions of N-H groups the blue colourations are distributed in different regions. The green colourations are found in the benzene ring which indicative of zero potential sites. With this study, one can justify, why binding affinity of a drug vary with the active sites receptor and why one drug is most reactive than other ones.

Mulliken atomic charges: The Mulliken atomic charges for all studied ligands were calculated by using DFT at B3LYP/6-311++G (d,p) level of theory and obtained data are tabulated in Table-3. For ligand **L1**, it observed that C_{22} is the most positive and C_{23} have the most negative charge. For ligand **L2**, the most positive charge is found in C_{20} and the most negative charge is found in C_{22}. For ligand **L3**, **L4** and **L5**, the most

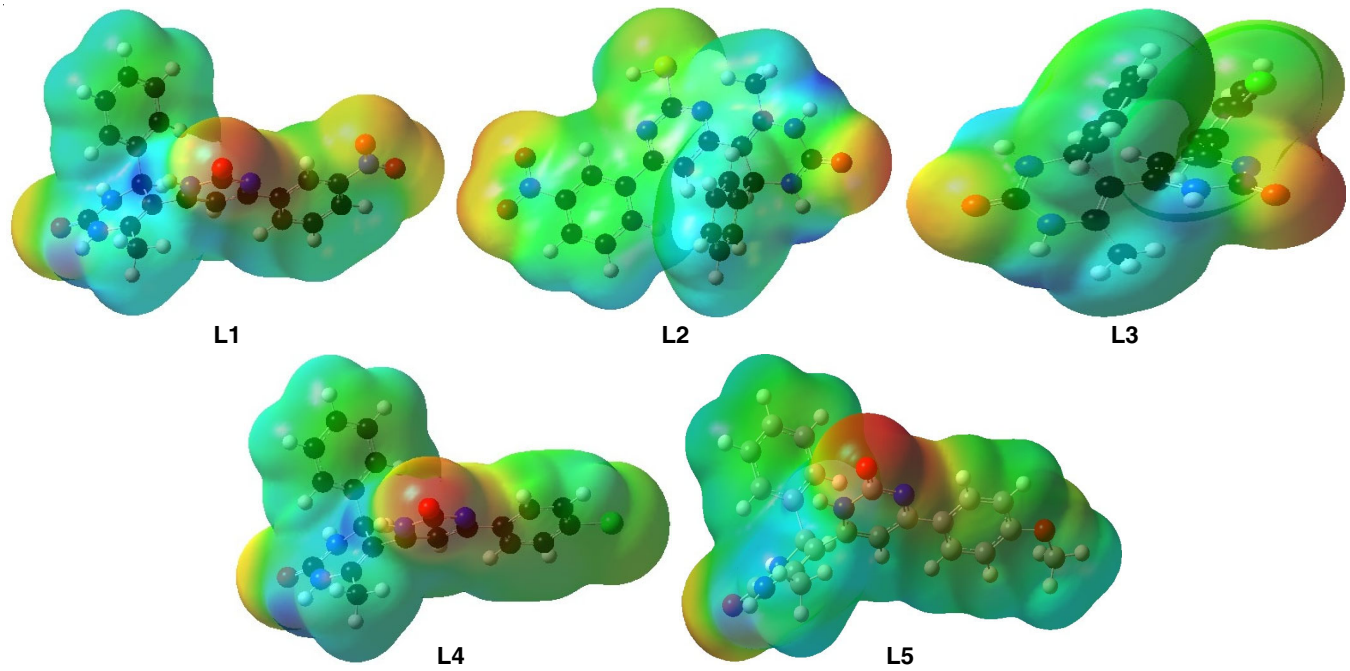

Fig. 3. Molecular electrostatic potential (MEP) maps of the studied ligands (**L1-L5**)

TABLE-3
MULLIKEN ATOMIC CHARGES OF THE STUDIED LIGANDS CALCULATED AT DFT/B3LYP/6-311++G (d,p) LEVEL OF THEORY

L1	L2	L3	L4	L5
1 C 0.631735	1 C 0.172166	1 C 0.305757	1 C 0.775457	1 C 0.573298
2 C 0.210643	2 C 0.193180	2 C 0.214517	2 C 0.209630	2 C 0.201605
3 C -0.501422	3 C 0.216417	3 C -0.442418	3 C -0.618049	3 C -0.574532
4 C 0.320024	4 C -0.643689	4 C 0.308720	4 C 0.330569	4 C 0.114625
5 C -0.745527	5 C 0.256244	5 C -1.033327	5 C -0.758671	5 C -0.765449
6 C -0.442379	6 C -0.283588	6 C -0.694154	6 C -0.203428	6 C 0.239380
7 H 0.149767	7 H -0.030604	7 H 0.195135	7 H 0.167784	7 H 0.137605
8 C 0.317095	8 C 0.303686	8 C 0.268026	8 C 0.320961	8 C 0.319265
9 O -0.322066	9 O -0.326325	9 O -0.324248	9 O -0.324533	9 O -0.326389
10 N -0.231316	10 N -0.279947	10 N -0.208523	10 N -0.235747	10 N -0.224835
11 H 0.318913	11 H 0.329172	11 H 0.320473	11 H 0.318992	11 H 0.317544
12 N -0.320481	12 N -0.318080	12 N -0.321857	12 N -0.315702	12 N -0.299396
13 H 0.359420	13 H 0.357102	13 H 0.359316	13 H 0.356125	13 H 0.355381
14 N -0.232125	14 N 0.139066	14 N -0.216905	14 N -0.238451	14 N -0.238550
15 H 0.335571	15 N 0.162976	15 H 0.326012	15 H 0.334995	15 H 0.337550
16 N -0.039419	16 C -0.787700	16 N -0.032455	16 N -0.065307	16 N -0.082487
17 O -0.309587	17 H 0.231768	17 O -0.315030	17 O -0.317583	17 O -0.322609
18 C -0.568614	18 H 0.203884	18 C -0.548643	18 C -0.575928	18 C -0.590535
19 H 0.196590	19 H 0.112635	19 H 0.193935	19 H 0.193696	19 H 0.193631
20 H 0.197304	20 C 1.537621	20 H 0.192557	20 H 0.197658	20 H 0.194427
21 H 0.177173	21 C -0.776629	21 H 0.174732	21 H 0.177143	21 H 0.176558
22 C 1.645706	22 C -0.871343	22 C 0.567873	22 C 0.589035	22 C 1.149707
23 C -1.151846	23 C -0.496775	23 C -0.405378	23 C -0.688279	23 C -0.359473
24 C -0.715002	24 H 0.103253	24 C 0.284238	24 C -0.372337	24 C -0.180160
25 C -0.604704	25 C -0.370426	25 C -0.345388	25 C -0.666423	25 C -0.280834
26 H 0.135193	26 H 0.284467	26 H 0.203448	26 H 0.130557	26 H 0.126222
27 C -0.164594	27 C 0.453874	27 C -0.207489	27 C -0.626609	27 C -0.417062
28 H 0.311507	28 H 0.198941	28 C -0.444345	28 H 0.229310	28 C -0.719499
29 C 0.381230	29 H 0.248773	29 H 0.176335	29 C 0.471713	29 H 0.200035
30 H 0.198131	30 N -0.194104	30 H 0.164491	30 H 0.202191	30 C -0.205324
31 H 0.247942	31 O 0.008652	31 C -0.023805	31 C -0.228448	31 H 0.240563
32 N -0.190182	32 O 0.013292	32 H 0.250471	32 H 0.239104	32 C 1.103612
33 O 0.007437	33 C -0.362403	33 C 1.017353	33 C 1.087528	33 C -0.200845
34 O 0.018632	34 H 0.288534	34 C -0.113724	34 C -0.155238	34 C -0.315341
35 C -0.173121	35 C 0.478572	35 C -0.244642	35 C -0.159697	35 C -0.448929
36 H 0.240742	36 C -0.181768	36 C -0.494424	36 C -0.535791	36 H 0.131343

37 C 1.084018	37 C -0.146109	37 H 0.127683	37 H 0.135483	37 C -0.364002
38 C -0.167961	38 C -0.382544	38 C -0.392030	38 C -0.522769	38 H 0.178924
39 C -0.170201	39 H 0.159037	39 H 0.178022	39 H 0.177282	39 C -0.355026
40 C -0.518417	40 C -0.229218	40 C -0.360494	40 C -0.268992	40 H 0.193415
41 H 0.140597	41 H 0.215349	41 H 0.193386	41 H 0.191319	41 H 0.185524
42 C -0.476673	42 C -0.347369	42 H 0.187379	42 H 0.183794	42 H 0.161432
43 H 0.176822	43 H 0.187446	43 H 0.159436	43 H 0.166332	43 H 0.230832
44 C -0.302353	44 H 0.192087	44 Cl 0.590612	44 Cl 0.487899	44 O -0.146166
45 H 0.192807	45 H 0.158815	45 H 0.209374	45 H 0.203424	45 C -0.336823
46 H 0.186460	46 S -0.257225	–	–	46 H 0.154654
47 H 0.166529	47 H 0.078834	–	–	47 H 0.153312
–	–	–	–	48 H 0.181452
–	–	–	–	49 H 0.202368

nucleophilic center is recognized on C_5, which is the most electrophilic susceptibility position and their respective nucleophilic susceptibility position visualized on C_{33}, C_{33} and C_{22}. From this study, it is possible to obtain a reasonable understanding about electronic charge distribution within a molecule and frontier molecular orbital approach.

Docking energy evaluation of the studied ligands: The non-bonding interactions of all ligands with the main protease showed that they interact with both catalytic residues (Cys145 and His41) identified by Autodock Vina, as shown in Fig. 4. All ligands show significant inhibitory potential by binding energy ranging from -8.1 to -8.8 kcal/mol. Table-4 revealed the binding affinity of our ligands with COVID-19 M^{pro}. These findings revealed that all ligands exhibit a good binding affinity for the target molecules and are stable inside the cavity. The formation of stable complexes resulting from the energetically favourable geometric arrangement of ligands in the active site, as well as the formation of hydrogen bonds, hydrophobic interactions and pi-sulfur interactions between them, could explain the inhibitory activity of the tested molecules against the COVID-19 virus (M^{pro}) protease. The results clearly show that ligands **L1** and **L2**, with binding energies of -8.8 kcal/mol and -8.6 kcal/mol, respectively, showed a significant inhibitory capacity for the main protease SARS-CoV-2, followed by **L4**, **L5** and **L3**.

TABLE-4
DOCKING RESULTS OF STUDIED LIGANDS (**L1-L5**) WITH SARS-CoV-2 M^{pro} USING AutoDock VINA

Entry	Binding affinity energy (kcal/mol)
L1	-8.8
L2	-8.6
L3	-8.1
L4	-8.3
L5	-8.2
Remdesivir	-7.2

Furthermore, remdesivir was selected as a standard drug that was docked against the targeted proteins. The results were compared to the studied ligands, indicating that they have a high affinity for the proteins. When compared to remdesivir, the selected ligands showed better and more appropriate binding interactions with the key amino acids of M^{pro}, including hydrogen bonds, hydrophobic bonds, halogen bonds, pi-alkyl, pi-pi and pi-sulfur interactions.

The interaction of ligand **L1** with SARS-CoV-2 M^{pro} showed the highest affinity interaction (Table-5) and forms hydrogen bonds between the oxygen of carbonyl group and hydrogen of THR25, the oxygen of nitro group with hydrogen of SER144 and HIS172 and the hydrogen of amide with the oxygen of HIS164 residues of the protein. The hydrophobic and pi-sulfur interactions with the corresponding amino acids LEU27, HIS41 and CYS145 are responsible for the high binding affinity. At the same time, ligand **L2** makes hydrogen bonds with THR25, SER144, HIS164 and GLU166. Other significant interactions are pi-pi stacked and π-alkyl inter-actions with HIS41, CYS 145, as well as pi-sulfur interactions with HIS41 and CYS145 (Fig. 4). On the other side, the complex with SARS-CoV-2 M^{pro} of ligand **L3** is formed by hydrogen bonding with SER46 and HIS164. Other interactions include hydrophobic interactions with HIS41, CYS145 and pi-sulfur interaction with MET49. When ligand **L4** is docked with 6Y2G, it forms two hydrogen bonds with THR25 and HIS164, four hydrophobic interactions with LEU27, HIS41, CYS145, one pi-sulfur and one halogen bond with MET49 and PHE140. The interaction between ligand **L5** and 6Y2G is characterized by hydrogen bonding with THR25, PHE140 and HIS164. Some of the hydrophobic and pi-sulfur have also been observed. The stability of the complex is aided by hydrophobic and pi-sulfur interactions with the residues of amino acids LEU27, HIS41, CYS145 and MET49. As illustrated in Fig. 5, the orbital picture of H-bonding and interaction clearly shows hydrogen bonding with both donor and acceptor regions, with the acceptor region being larger than the donor. These findings showed that docked ligands form a stable complex with targeted proteins (6Y2G), indicating that our selected ligands may have antiviral properties, with ligands **L1** and **L2** having a greater ability to inhibit the respective target protein than other compounds.

Conclusion

Five pyrimidine ring containing compounds have been investigated by molecular docking study and DFT calculations to assess their binding affinity towards the SARS-CoV-2 main protease (M^{pro}). To get insights about structure-reactivity of ligands, firstly, the optimization were performed, then the HOMO-LUMO orbital energies, thermodynamic parameters, electronic properties, MEPs and Mulliken atomic charges by using DFT at B3LYP method along with 6-311++G (d,p) basis set were calculated. The data obtained from molecular docking are compared with the FDA approved drugs remdesivir. These

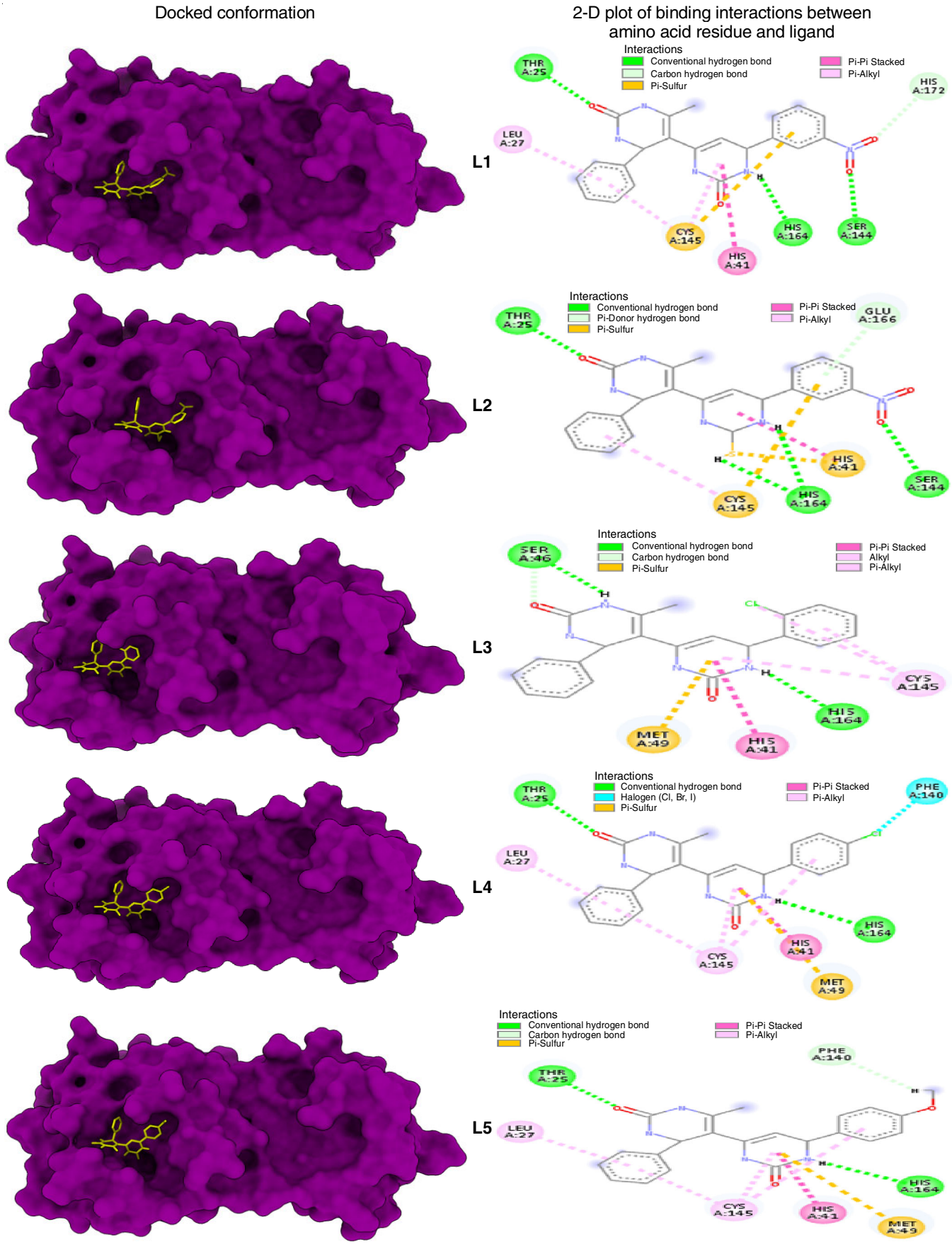

Fig. 4. Schematic representation for the docked conformation at the active site of the M^{pro} (PDB ID: 6Y2G) and 2D interaction between amino acid residue and ligands with M^{pro} (PDB ID: 6Y2G)

TABLE-5
NONCOVALENT INTERACTIONS OF LIGANDS WITH MAIN PROTEASE OF SARS-CoV-2 (POSE PREDICTED BY AutoDock VINA)

Drug candidate	Hydrogen bond (AA···Ligand)	Hydrophobic interaction (AA···Ligand)	Other	Halogen bond (AA···Ligand)
L1	THR25 (2.58684) O-H···O-C SER144 (2.72361) O-H···O-N HIS164 (2.72507) C-O···H-N HIS172 (2.8238) C-H···O-N	HIS41 (4.55456) Pi-Pi stacked CYS145 (5.39625) Pi-alkyl LEU27 (5.41984) Pi-alkyl CYS145 (5.26414) Pi-alkyl	CYS145 (5.2487) Pi-sulfur	
L2	THR25 (2.56834) O-H···O-C SER144 (2.84461) O-H···O-N HIS164 (2.68183) C-O···H-S HIS164 (2.72569) C-O···H-N GLU166 (2.95736) Pi-Donor	HIS41 (4.52465) Pi-Pi stacked CYS145 (5.28053) Pi-alkyl	CYS145 (5.27891) Pi-sulfur HIS41 (3.8811) Pi-sulfur	
L3	SER46 (2.39109) C-O···H-N HIS164 (2.22863) C-O···H-N SER46 (3.06712) C-H···O-C	HIS41 (4.43977) Pi-Pi stacked CYS145 (4.19278) alkyl CYS145 (5.20885) Pi-alkyl CYS145 (5.00423) Pi-alkyl	MET49 (5.27105) Pi-sulfur	
L4	THR25 (2.62904) O-H···O-C HIS164 (2.49868) C-O···H-N	HIS41 (4.35703) Pi-Pi stacked CYS145 (5.23486) Pi-alkyl CYS145 (5.04565) Pi-alkyl LEU27 (5.43533) Pi-alkyl CYS145 (5.47588) Pi-alkyl	MET49 (5.16599) Pi-sulfur	PHE140 (3.23995) Halogen (Cl, Br, I)
L5	THR25 (2.65711) O-H···O-C HIS164 (2.42281) C-O···H-N PHE140 (2.51371) C-O···H-C	HIS41 (4.36462) Pi-Pi stacked CYS145 (5.15535) Pi-alkyl LEU27 (5.38767) Pi-alkyl CYS145 (5.37385) Pi-alkyl CYS145 (5.05288) Pi-alkyl	MET49 (5.27917) Pi-sulfur	

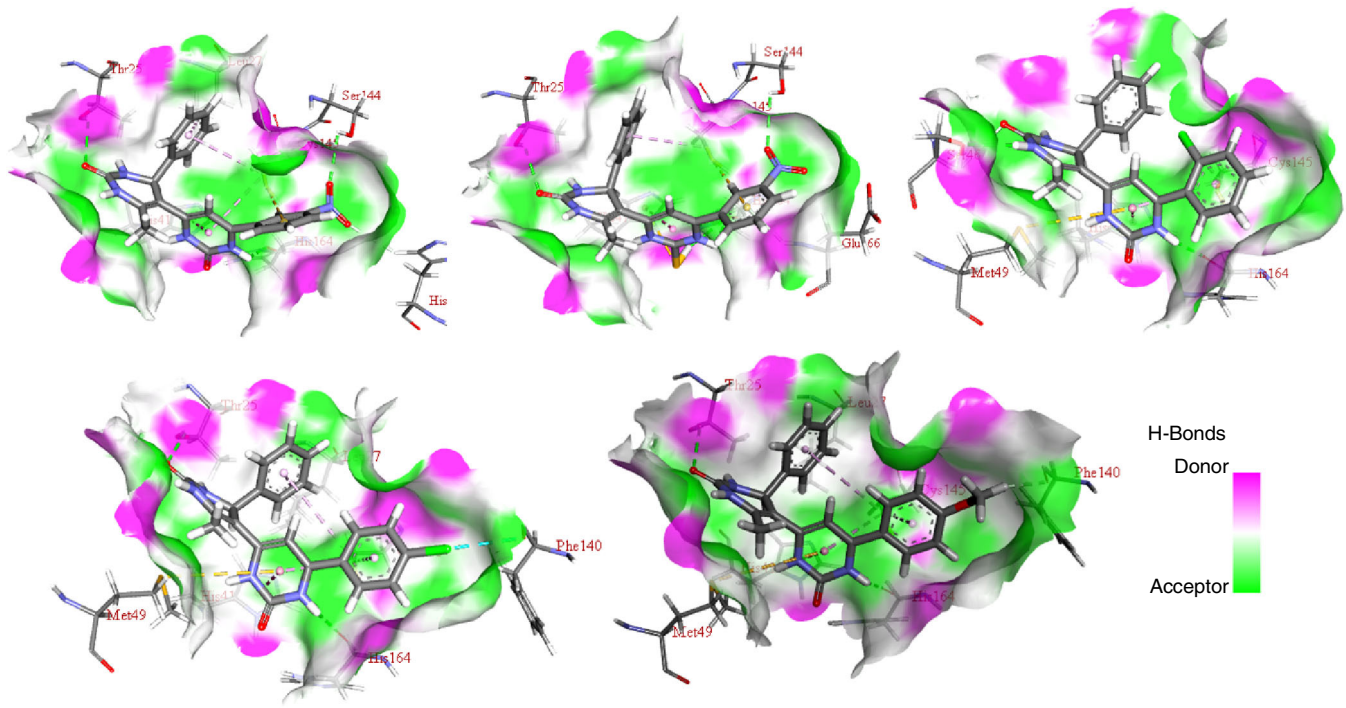

Fig. 5. 3D H bonding between amino acid residue and ligands with M^{pro} (PDB ID: 6Y2G)

findings demonstrated that all of the selected ligands formed stable complexes with the targeted proteins and had a higher binding affinity than remdesivir. The calculated HOMO and LUMO energies, reactivity descriptors as well as thermal parameters and demonstrated charge transfer within molecule, allows us to find the most reactive ligands against the COVID-19 virus. According to quantum chemical studies, ligand **L1** (3.26 eV) and ligand **L2** (3.53 eV) demonstrated lower HOMO-LUMO energy gaps and predicted better chemical reactivity. The current results can provide useful insight for the development of pyrimidine derivatives with improved antiviral activity.

ACKNOWLEDGEMENTS

The authors are grateful to the Synthetic and Computational Chemistry Research Group, Department of Chemistry, Mawlana

Bhashani Science & Technology University for their guidance and opportunity provided to perform the research.

CONFLICT OF INTEREST

The authors declare that there is no conflict of interests regarding the publication of this article.

REFERENCES

1. D.S. Hui, E. I Azhar, T.A. Madani, F. Ntoumi, R. Kock, G. Ippolito, O. Dar, T.D. Mchugh, Z.A. Memish, C. Drosten, A. Zumla and E. Petersen, *Int. J. Infect. Dis.*, **91**, 264 (2020); https://doi.org/10.1016/j.ijid.2020.01.009
2. A. Sharma, S. Tiwari, M.K. Deb and J.L. Marty, *Int. J. Antimicrob. Agents*, **56**, 106054 (2020); https://doi.org/10.1016/j.ijantimicag.2020.106054
3. R.K. Mohapatra, M.M. El-ajaily, F.S. Alassbaly, A.K. Sarangi, D. Das, A.A. Maihub, S.F. Ben-Gweirif, A. Mahal, M. Suleiman, L. Perekhoda, M. Azam and T.H. Al-Noor, *Chem. Pap.*, **75**, 1005 (2021); https://doi.org/10.1007/s11696-020-01342-8
4. R.K. Mohapatra, P.K. Das and V. Kandi, *Diabetes Metab. Syndr.*, **14**, 1593 (2020); https://doi.org/10.1016/j.dsx.2020.08.024
5. J. Liang, C. Karagiannis, E. Pitsillou, K.K. Darmawan, K. Ng, A. Hung and T.C. Karagiannis, *Comput. Biol. Chem.*, **89**, 107372 (2020); https://doi.org/10.1016/j.compbiolchem.2020.107372
6. K. Kapusta, S. Kar, J.T. Collins, L.M. Franklin, W. Kolodziejczyk, J. Leszczynski and G.A. Hill, *J. Biomol. Struct. Dyn.*, **39**, 6810 (2021); https://doi.org/10.1080/07391102.2020.1806930
7. S. Chidambaram, M.A. El-Sheikh, A.H. Alfarhan, S. Radhakrishnan and I. Akbar, *Saudi J. Biol. Sci.*, **28**, 1100 (2021); https://doi.org/10.1016/j.sjbs.2020.11.038
8. I. Achilonu, E.A. Iwuchukwu, O.J. Achilonu, M.A. Fernandes and Y. Sayed, *J. Mol. Graph. Model.*, **101**, 107730 (2020); https://doi.org/10.1016/j.jmgm.2020.107730
9. A. El-Demerdash, A.A. Al-Karmalawy, T.M. Abdel-Aziz, S.S. Elhady, K.M. Darwish and A.H.E. Hassan, *RSC Adv.*, **11**, 31339 (2021); https://doi.org/10.1039/D1RA05817G
10. K.A. Peele, C.P. Durthi, T. Srihansa, S. Krupanidhi, V.S. Ayyagari, D.J. Babu, M. Indira, A.R. Reddy and T.C. Venkateswarulu, *Inform. Med. Unlocked*, **19**, 100345 (2020); https://doi.org/10.1016/j.imu.2020.100345
11. M. E. Sobhia, G. S. Kumar, S. Sivangula, K. Ghosh, H. Singh, T. Haokip and J. Gibson, *Future Med. Chem.*, **13**, 1435 (2021); https://doi.org/10.4155/fmc-2020-0264
12. Z. Abdelrahman, M. Li and X. Wang, *Front. Immunol.*, **11**, 552909 (2020); https://doi.org/10.3389/fimmu.2020.552909
13. U. Bacha, J. Barrila, A. Velazquez-Campoy, S.A. Leavitt and E. Freire, *Biochem.*, **43**, 4906 (2004); https://doi.org/10.1021/bi0361766
14. F.A.D.M. Opo, M.M. Rahman, F. Ahammad, I. Ahmed, M.A. Bhuiyan and A.M. Asiri, *Sci. Rep.*, **11**, 4049 (2021); https://doi.org/10.1038/s41598-021-83626-x
15. J.L. Araújo, L.A. de Sousa, A.O. Sousa, R.S. Bastos, G.T. Santos, M.R. Lage, S.R. Stoyanov, I.N.G. Passos, R.B. de Azevedo and J.A. Rocha, *J. Braz. Chem. Soc.*, **32**, 1628 (2021); https://dx.doi.org/10.21577/0103-5053.20210061
16. B. Gogoi, P. Chowdhury, N. Goswami, N. Gogoi, T. Naiya, P. Chetia, S. Mahanta, D. Chetia, B. Tanti, P. Borah and P.J. Handique, *Mol. Divers.*, **25**, 1963 (2021); https://dx.doi.org/10.1007/s11030-021-10211-9
17. R. Carrasco-Velar, J.A. Padron and J. Galvez, *J. Pharm. Pharm. Sci.*, **7**, 19 (2004).
18. V.R. Murthy, D.V. Raghuram and P.N. Murthy, *Bioinformation*, **2**, 12 (2007); https://dx.doi.org/10.6026/97320630002012
19. M.F. Costa, *Ciencias exatas e tecnologicas. Londrina*, **31**, 31 (2010); https://doi.org/10.5433/1679-0375.2010v31n1p31
20. M.J. Frisch, G.W. Trucks, H.B. Schlegel, G.E. Scuseria, M.A. Robb, J.R. Cheeseman, G. Scalmani, V. Barone, B. Mennucci, G.A. Petersson, H. Nakatsuji, M. Caricato, X. Li, H.P. Hratchian, A.F. Izmaylov, J. Bloino, G. Zheng, J.L. Sonnenberg, M. Hada, M. Ehara, K. Toyota, R. Fukuda, J. Hasegawa, M. Ishida, T. Nakajima, Y. Honda, O. Kitao, H. Nakai, T. Vreven, J.A. Montgomery Jr., J.E. Peralta, F. Ogliaro, M. Bearpark, J.J. Heyd, E. Brothers, K N. Kudin, V.N. Staroverov, R. Kobayashi, J. Normand, K. Raghavachari, A. Rendell, J.C. Burant, S.S. Iyengar, J. Tomasi, M. Cossi, N. Rega, J.M. Millam, M. Klene, J.E. Knox, J.B. Cross, V. Bakken, C. Adamo, J. Jaramillo, R. Gomperts, R.E. Stratmann, O. Yazyev, A.J. Austin, R. Cammi, C. Pomelli, J.W. Ochterski, R.L. Martin, K. Morokuma, V.G. Zakrzewski, G.A. Voth, P. Salvador, J.J. Dannenberg, S. Dapprich, A.D. Daniels, Ö. Farkas, J.B. Foresman, J.V. Ortiz, J. Cioslowski and D.J. Fox, Gaussian 09, Revision E.01, Gaussian, Inc., Wallingford CT (2009).
21. C. Lee, W. Yang and R.G. Parr, *Phys. Rev. B Condens. Matter*, **37**, 785 (1988); https://doi.org/10.1103/PhysRevB.37.785
22. A.D. Becke, *J. Chem. Phys.*, **98**, 5648 (1993); https://doi.org/10.1063/1.464913
23. H. Vural and I. Uçar, *J. Coord. Chem.*, **69**, 3010 (2016); https://doi.org/10.1080/00958972.2016.1225042
24. S. Azhagiri, S. Jayakumar, S. Gunasekaran and S. Srinivasan, *Spectrochim. Acta A Mol. Biomol. Spectrosc.*, **124**, 199 (2014); https://doi.org/10.1016/j.saa.2013.12.106
25. R. Dennington, T.A. Keith and J.M. Millam, GaussView, Version 6, Semichem Inc., Shawnee Mission, KS (2016).
26. O. Trott and A.J. Olson, *J. Comput. Chem.*, **31**, 455 (2010); https://doi.org/10.1002/jcc.21334
27. W.L. DeLano, The PyMOL Molecular Graphics System, Delano Scientific, San Carlos, USA (2002).
28. L. Zhang, D. Lin, X. Sun, U. Curth, C. Drosten, L. Sauerhering, S. Becker, K. Rox and R. Hilgenfeld, *Sci.*, **368**, 409 (2020); https://doi.org/10.1126/science.abb3405
29. N. Guex and M.C. Peitsch, *Electrophoresis*, **18**, 2714 (1997); https://doi.org/10.1002/elps.1150181505
30. T.D. Goddard, C.C. Huang, E.C. Meng, E.F. Pettersen, G.S. Couch, J.H. Morris and T.E. Ferrin, *Protein Sci.*, **27**, 14 (2018); https://doi.org/10.1002/pro.3235
31. M.A. Jordaan, O. Ebenezer, N. Damoyi and M. Shapi, *Heliyon*, **6**, e04642 (2020); https://doi.org/10.1016/j.heliyon.2020.e04642
32. A. Semeniuk, J. Kalinowska-Tluscik, W. Nitek and B.J. Oleksyn, *J. Chem. Crystallogr.*, **38**, 333 (2008); https://doi.org/10.1007/s10870-008-9327-9
33. E. Eroglu and H. Türkmen, *J. Mol. Graph. Model.*, **26**, 701 (2007); https://doi.org/10.1016/j.jmgm.2007.03.015
34. S. LaPointe and D. Weaver, *Curr. Comput. Aided Drug Des.*, **3**, 290 (2007); https://doi.org/10.2174/157340907782799390
35. A.M. Ferreira, M. Krishnamurthy, B.M. Moore II, D. Finkelstein and D. Bashford, *Bioorg. Med. Chem.*, **17**, 2598 (2009); https://doi.org/10.1016/j.bmc.2008.11.059
36. N.C. Garbett and J.B. Chaires, *Expert Opin. Drug Discov.*, **7**, 299 (2012); https://doi.org/10.1517/17460441.2012.666235
37. G.W. Ejuh, C. Fonkem, Y.T. Assatse, R.A. Yossa Kamsi, T. Nya, L.P. Ndukum, J.M.B. Ndjaka, *Heliyon*, **6**, e04647 (2020); https://doi.org/10.1016/j.heliyon.2020.e04647
38. R.G. Parr, L.V. Szentpaly and S. Liu, *J. Am. Chem. Soc.*, **121**, 1922 (1999); https://doi.org/10.1021/ja983494x